Eur. Phys. J. Plus (2024) 139:453
https://doi.org/10.1140/epjp/s13360-024-05258-0

THE EUROPEAN PHYSICAL JOURNAL PLUS

Regular Article

Thermal Aspects and Joule–Thomson Expansion of ModMax Black Hole

M. R. Shahzad[1,a], **R. H. Ali**[2,b], **G. Abbas**[2,c], **Wen-Xiu Ma**[3,4,5,6,d]

[1] Department of Mathematics, Bahauddin Zakariya University, Vehari Campus, Vehari 61100, Pakistan
[2] Department of Mathematics, The Islamia University of Bahawalpur, Bahawalpur, Pakistan
[3] Department of Mathematics, Zhejiang Normal University, Jinhua 321004, Zhejiang, China
[4] Department of Mathematics, King Abdulaziz University, Jeddah 21589, Saudi Arabia
[5] Department of Mathematics and Statistics, University of South Florida, Tampa, FL 33620-5700, USA
[6] Material Science Innovation and Modeling, Department of Mathematical Sciences, North-West University, Mafikeng Campus, Mmabatho 2735, South Africa

Received: 21 December 2023 / Accepted: 8 May 2024

Abstract This paper analyzes the thermal characteristics and Joule–Thomson adiabatic expansion of the AdS ModMax black hole immersed with a nonlinear electrodynamic field. The obtained solution of the AdS ModMax black hole is employed to evaluate thermodynamic variables, e.g., geometric mass, black hole temperature, entropy, heat capacity, and free energy. The study of the equation of state and the extended phase space shows rich phase behavior, especially in P–V criticality, exhibiting first and second-order phase transitions. The critical points reveals the critical exponents, demonstrating that critical behavior explains the universal characteristics. The effect of coupling parameter and thermal comparative analysis of AdS ModMax black hole with well-known black holes is also present. The process of Joule–Thomson adiabatic expansion of AdS ModMax black hole also investigated to obtain the inversion and isenthalpic curves. The cooling and heating phase transitions occur by diminishing the Joule–Thomson coefficient. Finally, we calculate the ratio of minimum inversion temperature to critical temperature and compare it with some well-known black holes.

1 Introduction

In the early twentieth century, Albert Einstein proposed a novel framework for interpreting the general theory of relativity (GTR), which transformed Newton's universal gravitational theory. Initially, Schwarzschild successfully inculcate an exact solution to a static black hole (BH), which was derived from the Einstein's field equations. At the same time, theoretical physicists formulated an alternative, precise solution that epitomize the space-time configuration possessing both mass and charge for spherical symmetry [1–4]. Subsequently, the Reissner–Nordstrom (RN) BH solution, which is illustrious for its salient effects on theoretical physics, has remarkable stability properties as well as super-symmetry within the framework of super-gravity [5]. With the improvement of the BH metrics over time, the understanding of BHs has become a fascinating subject. The direct observation of BHs through X-ray, light, or other electromagnetic radiation remains ambiguous, the presence of these enigmatic entities can be observed by their insightful impact on surrounding matter.

In the past few decades, BH thermodynamics has emerged as a captivating and astonishing subject in cosmology and physics to unveil the mysterious traits of a BH. Black hole thermodynamics has significant enlightening relations between classical gravitational theory and quantum gravity theory. In the innovative research of Bekenstein and Hawking [6–8], the entropy and BH radiation are specified as their horizon area and surface gravity. In light of these results, numerous investigations have been initiated to understand the principles governing thermodynamics [9–14]. The thermodynamical analysis of the Schwarzschild BH and the RN-BH surrounded by quintessence matter fields have been studied in [15, 16], respectively. Subsequently, Bardeen [17] and other researchers [18–21] have studied the thermodynamical properties of different BHs.

In the quantum GR, the issue of singularities has been a source of debate, which was dealt by Penrose and Hawking [22, 23]. Different kinds of corrections to identify regular (nonsingular) BHs were developed by Sakharov [24] and Gliner [25] to address the problem of singularity [26–30]. The Einstein field equations for suitable nonlinear electrodynamics (NLED) fields [31–35] have been used to find many of the BH solutions. The concept of quantum correction [36–41] in BH entropy has brought significant

[a] e-mails: dr.rizwanshahzad@bzu.edu.pk; rezwan.chaudhery@gmail.com
[b] e-mail: hasnainali408@gmail.com
[c] e-mail: ghulamabbas@iub.edu.pk
[d] e-mail: mawx@cas.usf.edu (corresponding author)

Published online: 29 May 2024

interest to the astrophysicist community in recent years. Numerous articles have been published to unveil the thermodynamics of different NLED BHs [42–53]. Instead of GR, various modified theories are used to investigate BH thermodynamics and phase transitions (see [54–61] and references therein).

Black holes have been further studied in first and second-order extended-phase space, Joule–Thomson (J–T) expansion, and heat engines. In classical mechanics, the process of shifting fluids from a high-pressure zone to a low-pressure zone is referred to as J–T expansion (or J–T effects). It exhibits extensive applications in the realm of thermal mechanics, encompassing heat pumps and air conditioning systems. Okcu and Aydyner were the pioneering astrophysicists who introduced the innovative study [62] to investigate the influence of the J–T effects on AdS-charged BHs. Furthermore, the AdS Kerr BH [63], AdS-charged BHs in the *f(R)* gravity [64], and the K-dimensional AdS-charged BH [65] are also of great interest to explore the fascinating traits of J–T expansion in the field of astrophysics. This thriving subject (J–T expansion) governs the great attention to obtain the more interesting features of different black holes [66–73]. Recently, the investigation of various types of charged BHs in different gravitational theories [74–81] have been studied to reveal the more mysterious J–T effects.

The NLED arises from the Maxwell's theory, specifically in the domain of extreme conditions characterized by intense field strengths. The exploration of NLED has revealed that the study of BH physics [82–88] has the capacity to construct regular solutions to BHs. The impacts of NLED in J–T expansion were also observed in [89–91]. The classical theories are characterized by Lagrangians that exhibit nonlinearity in the two electromagnetic invariants in astrophysics: the Euler-Heisenberg (EH) theory and the Born–Infeld (BI) theory. Both the EH NLED and the BI NLED have electric-magnetic duality invariance, which reduces to Maxwell electrodynamics in the weak field regime because of the fixed energy scale interactions that break the conformal invariance. The QED Lagrangian has derived the EH NLED from the tree-level approximation and phenomenologically reveals the effect of vacuum polarization. In BI NLED, the self-energy of charges is finite and the BI theory solves the divergence of the self-energy of point particles. Moreover, the effective action of BI NLED can also be derived from open super-strings at low energy dynamics of D-branes without any physical singularities. Recently, an NLED theory with two symmetries has been proposed [92], and this theory is characterized by a dimensionless parameter γ, and in the case where $\gamma = 0$, it reduces to the Maxwell's theory. This modified Maxwell theory, commonly called ModMax NLED theory, sparked analysis of various domains, including classical solutions [93, 94] as well as super-symmetric investigations [95–102]. ModMax electrodynamics have been comprehensively explored and discussed by many esteemed researchers [103–115].

With all the factors mentioned above, we are encouraged to conduct studies on the thermodynamics of spherically symmetric charged ModMax BH [116], as well as P–V criticality, critical exponents, and J–T expansions. The following is the arrangement of the paper: In Sect. 2, we present the review of a static solution for the spherically symmetric charged MaxMod BH [116]. The Sect. 3 focuses on analyzing the thermodynamic properties of BH. In Sect. 4, we derive the extended thermodynamics approach for critical exponents. The Sect. 5 of this paper examines the concepts of J–T expansion, inversion temperature, and cooling-heating regions. The final section presents the discussion and concluding remarks.

2 Review of nonlinear electrodynamic BH solution

The ModMax NLED exhibits the fundamental symmetries of Maxwell's equations, namely conformal invariance and SO(2) duality-rotation invariance. The derivation of the ModMax NLED Lagrangian in [117] involved utilization of the Bessel-Hagen criterion to ensure conformal invariance while also incorporating the Gaillard-Zumino criterion to guarantee invariance under duality transformations. The metric function of spherically symmetric AdS charged ModMax BH [117],

$$ds^2 = -N(r)dt^2 + \frac{1}{N(r)}dr^2 + r^2 d\Omega_2^2, \tag{1}$$

where,

$$N(r) = 1 - \frac{2M}{r} + \frac{Q^2 \exp(-\eta)}{r^2} - \Lambda \frac{r^2}{3}. \tag{2}$$

If $\gamma = \Lambda = 0$, it reduces to the RN-BH and if $Q = \Lambda = 0$, then it is nothing but reveals the Schwarzschild BH. By replacing the cosmological constant Λ with the AdS length scale l is a convenient choice, particularly when dealing with BH solutions in the context of AdS space and its dual conformal field theories. So, AdS space is a maximally symmetric solution to EEs with a negative cosmological constant. The cosmological constant is provided $-\Lambda = \frac{3}{l^2}$. The BH radius of the Modmax AdS-BH [117] computed as $N(r_+) = 0$, for the real largest root as

$$1 - \frac{2M}{r_+} + \frac{Q^2 \exp(-\eta)}{r_+^2} + \frac{r_+^2}{l^2} = 0. \tag{3}$$

The conduct of the solution for a fixed value of η is presented in Fig. 1a, b for varying the value of charge Q. It is manifested that as the charge Q increases, the horizon radius decreases. We observe that a naked singularity appears at $Q = 1.2$ for RN-BH, indicating no event horizon, hence no BH, while Schwarzschild BH shows one root and our studied Modmax AdS-BH represents

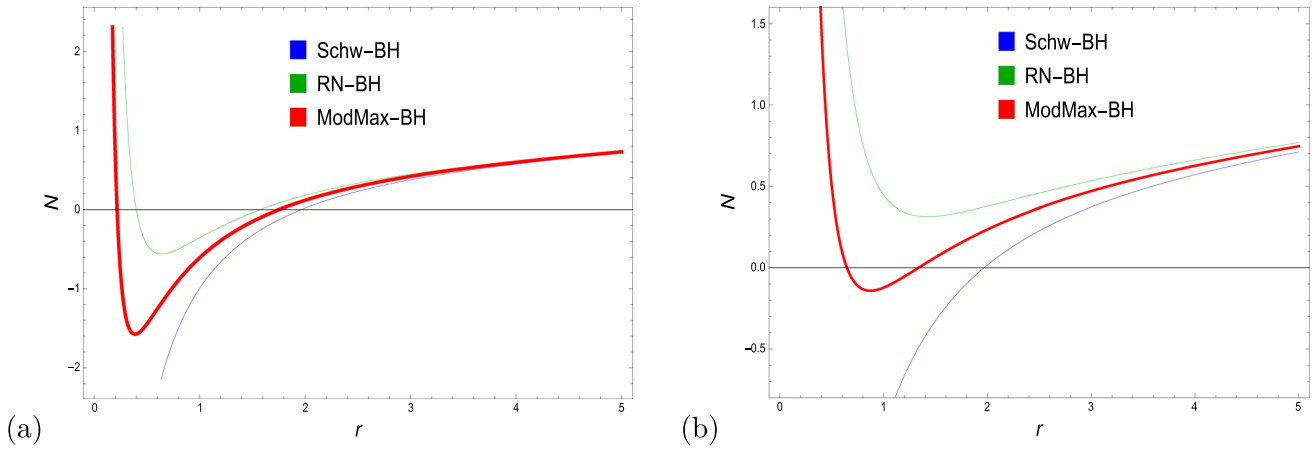

Fig. 1 Evolution of N along r_+ by taking $l = 15$, $M = 1$, and $\eta = 0$, $Q = 0$ represents Schwarzschild BH (blue curve), green curve represents RN-BH with $\eta = 0$ and $Q \neq 0$ and red curve denotes the ModMax BH for which $\eta \neq 0$ and $Q \neq 0$ **a** for $Q = 0.80$, $\eta = 0.50$ **b** for $Q = 1.20$ and $\eta = 0.50$

two roots. In Fig. 1a, the horizon radius of RN-BH is smaller than the ModMax BH, which is smaller than that of the Schwarzschild BH. In Fig. 1b, RN-BH has no horizon radius and the horizon radius of ModMax BH is smaller than the Schwarzschild BH.

3 Thermodynamic quantities of ModMax Black Hole

This section deals with some thermodynamical characteristics of Modmax-AdS BH [117]. The giant contribution of Hawking and Bekenstein provide a significant justification for the thermodynamical features of BHs [6, 7]. We can determine the mass of BH using $N(r_+) = 0$.

$$M = \frac{Q^2 \exp(-\eta)}{2r_+} + \frac{r_+^3}{2l^2} + \frac{r_+}{2}. \tag{4}$$

If $\eta \to 0$, and $Q = 0$, it reduces to the mass of RN BH [13] and Schwarzschild BH [7], respectively.

Figure 2 represents the geometrical mass of the ModMax AdS BH with r_+. The mass of the considered BH is graphically depicted and observed for both, the charged parameter Q and the coupling parameter η. From Fig. 2a, it is identified that the BH mass drops to minimal for the small horizon radius at $r_+ < 1$ and gradually rises to its maximal for the large horizon radius at $r_+ = 7$, so we conclude that BH mass rises with increasing the BH radius. As per the charge parameter Q, the mass of the considered BH increases with increase in the charge parametric values of Q and reaches its peak at $Q = 2.5$. There are opposite effects of η on the mass of ModMax AdS BH, with the BH mass minimum at $\eta = 2.5$, as can be observed in Fig. 2b. In Fig. 2c, we discussed the comparative study of ModMax BH (red line) with the RN-BH (green line) and Schwarzschild BH (blue line) and revealed that the mass of our considered BH is maximum as compared to the RN and Schwarzschild BHs.

Further, Hawking and Bekenstein discussed the complete independent solution which is known as Hawking temperature. Hawking [8], argued that each BH emits thermal radiations which is proportional to its surface gravity κ. The Hawking temperature can be computed as $T = \frac{\kappa}{2\pi}$. By applying the Eqs. (2), and (4), it takes the form

$$T = -\frac{Q^2 \exp(-\eta)}{4\pi r_+^3} + \frac{3r_+}{4\pi l^2} + \frac{1}{4\pi r_+}. \tag{5}$$

If $\eta = 0$ and $Q = 0$, then it lapses back to the Hawking temperature of RN BH [13] and Schwarzschild BH [7], respectively.

The physical profile of the Hawking temperature for the considered BH with respect to horizon radius r_+ is displayed in Fig. 3. Initially, for the small BH radii, a phase transition occurs from an unstable thermodynamical system to a stable thermodynamical system and shows increasing behavior throughout the given domain. We deal with the Hawking temperature for both parametric entities, such as Q, and η. From Fig. 3a, it is noted that the Hawking temperature grows to its maximum for the smallest charge parametric value $Q = 0.5$ and the minimum temperature at the largest value of $Q = 2.5$. Moreover, the increasing behavior of Hawking temperature for the smallest charge parametric value at $Q = 0.5$, remain maximum throughout the given domain of the horizon radius. Hence, both small and large radii maintain stability in the system. From Fig. 3b, the coupling constant parameter determines the opposite behavior as we discussed in Fig. 3a. The comparative study of the Hawking temperature of our considered AdS ModMax BH with the other two important BHs, such as RN BH and Schwarzschild BH, is revealed in Fig. 3c. We are able to deduce, based on the information shown in Fig. 3c, that the Hawking temperature for the AdS ModMax BH (the red line) is the lowest possible value when compared to the RN BH [13] (the green line) and the Schwarzschild BH [7] (the blue line).

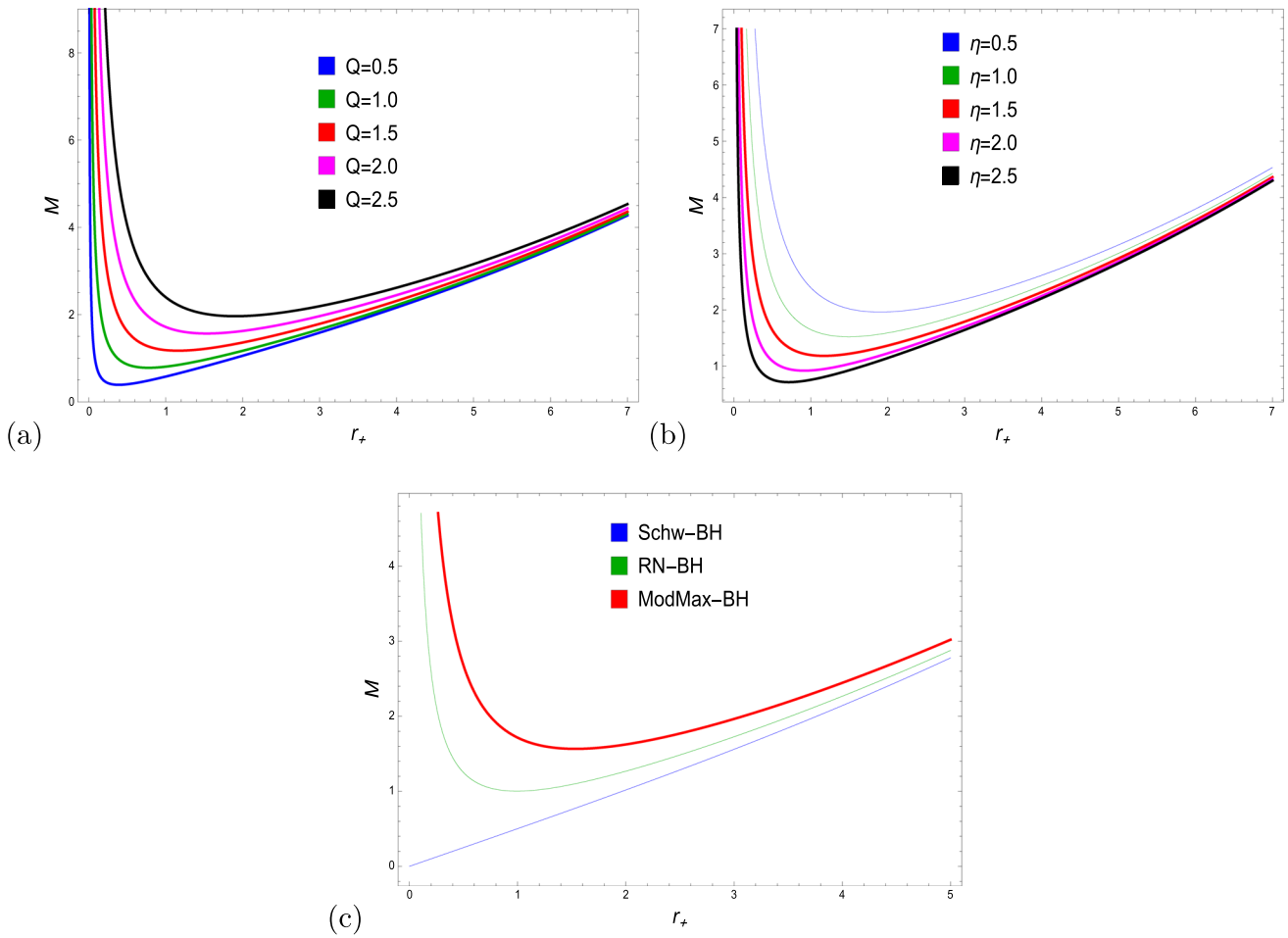

Fig. 2 Evolution of M along r_+ by taking $l = 15$, **a** $\eta = 0.50$ for different values of Q **b** for $Q = 2.50$ and different values of η and **c** represents the comparative analysis of the behavior of mass function for Schwarzschild BH (blue curve) with $\eta = 0$, $Q = 0$, RN-BH (green curve) with $\eta = 0$ and $Q \neq 0$ and red curve denotes the ModMax BH for which $\eta \neq 0$ and $Q \neq 0$

The BH entropy is derived from the first law of thermodynamics as

$$S = \int \left(\frac{1}{T} dM\right) dr_+, \tag{6}$$

$$S = \pi r_+^2. \tag{7}$$

In order to reveal the local stability of the considered BH system, heat capacity can be computed as $C = \left(\frac{\partial M}{\partial r_+}\right)\left(\frac{\partial r_+}{\partial T}\right)$,

$$C = \frac{2\pi r_+^2\left(l^2 r_+^2 \exp(-\eta) + 3r_+^4 \exp(\eta) - l^2 Q^2\right)}{-l^2 r_+^2 \exp(\eta) + 3r_+^4 \exp(\eta) + 3l^2 Q^2}. \tag{8}$$

In order to achieve this purpose, we direct our attention towards the BH stability, which is indicated by its heat capacity. The heat capacity's behavior determines the BH's thermodynamic local stability. If C is greater than zero, the thermodynamical system exhibits local stability, whereas it experiences instability when the specific heat C is less than zero. To determine the stability, we analyze Fig. 4 for different amounts of Q and η. The discontinuity appears at $r_+ = r_c$, corresponding to the maximum temperature. Figure 4a, b demonstrate the discontinuity at critical values. As the charge Q increases, the critical radius also increases. In Fig. 4a, b express the stability for small radius and change this phase of stability to instability for large radii with varying Q for fixed values of η in Fig. 4a and the same behavior can be observed in Fig. 4b for fixed value of Q and altered values of η. In comparison to small BHs, the presence of Q and η tends to place large BHs in the unstable region. In Fig. 4c we present a comparative study of well known Schwarzschild BH and RN BH with our newly studied ModMax BH. It can be examined that Schwarzschild BH remain in the unstable phase throughout the BH radius and RN BH persists in the stable region for small value of r_+ and shows transition to unstable region for large horizon radius. In comparison to both (i.e., Schwarzschild BH and RN BH), the ModMax BH remain in the stable region for large value of horizon radius.

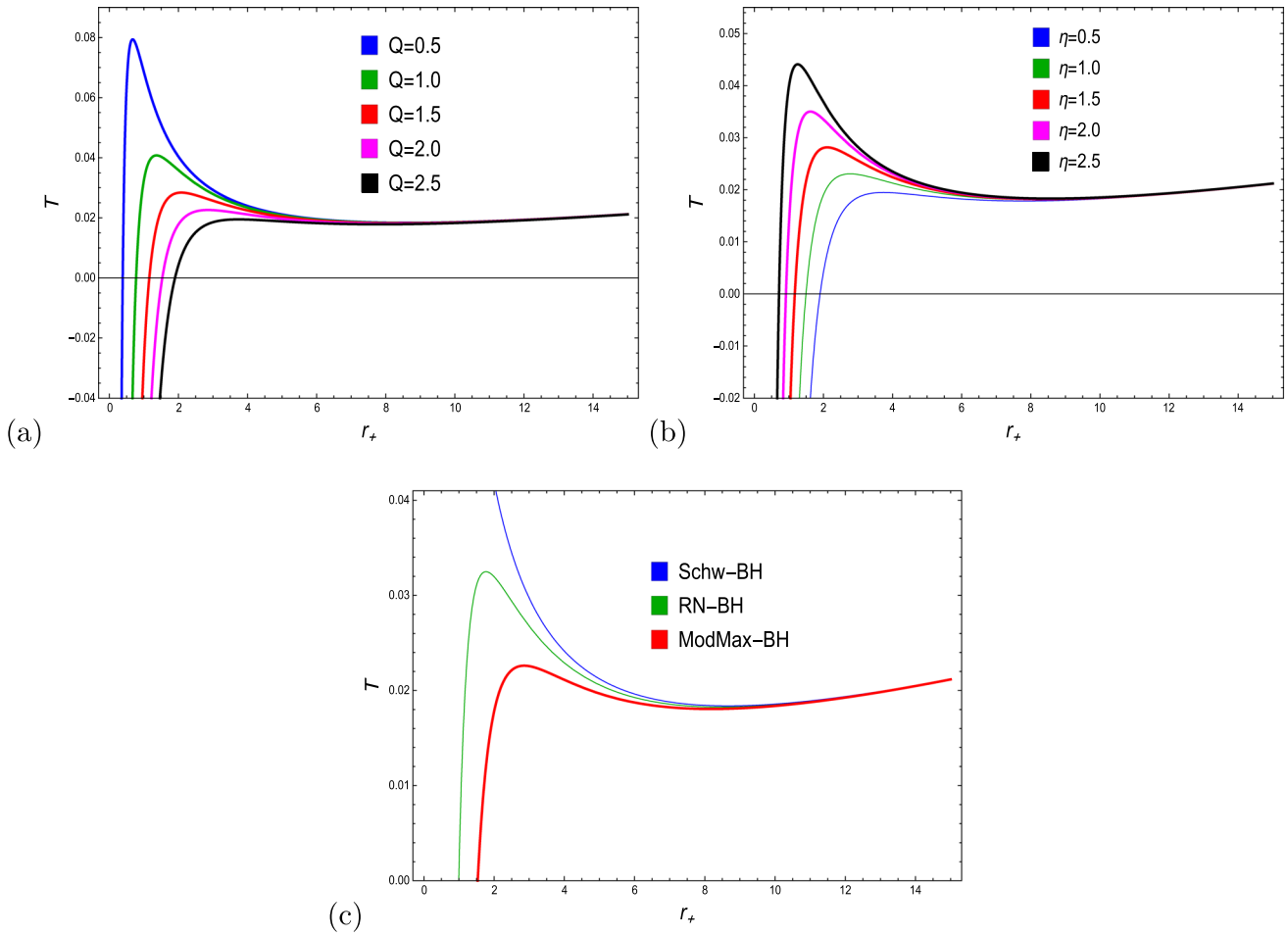

Fig. 3 Evolution of Hawking temperature T along r_+ by taking $l = 15$, **a** $\eta = 0.50$ for different values of Q **b** for $Q = 2.50$ and different values of η and **c** represents the comparative analysis of the behavior of Hawking temperature T for Schwarzschild BH (blue curve) with $\eta = 0$, $Q = 0$, RN-BH (green curve) with $\eta = 0$ and $Q \neq 0$ and red curve denotes the ModMax BH for which $\eta \neq 0$ and $Q \neq 0$

To evaluate the Gibbs free energy (GFE), we must analyze the global stability of the provided BH thermodynamic system. To determine the global stability of the system, one must calculate the value of $G = M - TS$.

$$G = \frac{Q^2 r^2 \exp(-\eta)}{4r_+^3} + \frac{Q^2 \exp(-\eta)}{2r_+} - \frac{3r^2 r_+}{4l^2} + \frac{r_+^3}{2l^2} - \frac{r^2}{4r_+} + \frac{r_+}{2}. \tag{9}$$

The confirmation of global stability is achieved when the condition $G \leq 0$ is satisfied. In order to investigate the dynamics of this expression, we proceed by constructing a graphical representation given in Fig. 5. In this observation, we discern the presence of a local minimum ($r_{\min}$) and local maximum ($r_{\max}$) which are in good concurrent with the extremal points of Hawking temperature. In the current epoch, the local transformative nature of free energy change is observed. Beyond the threshold denoted as $r_{\min}$, the free energy exhibits a progressive augmentation in correspondence with the expansion of the horizon radius, reaching its utmost magnitude at $r_{\max}$. Beyond this juncture, free energy exhibits a gradual decline with increasing horizon radius. It is noteworthy to observe the impact of the BH parameters on the global stability. We observe the impact of Q and η by observing that, as the value of Q rises, the free energy also rises (Fig. 5a), and the free energy falls with the rising value of η (Fig. 5b). We conclude that the stability achieve its maximum value at the large value of charge parameter Q with smaller value of η.The comparative analysis of free energy for the well known Schwarzschild BH and RN BH with ModMax BH is presented in Fig. 5c. we revealed that Schwarzschild BH has the the least free energy throughout the BH radius as compared to RN BH and ModMax BH, while the ModMax BH achieve the large amount of free energy in comparison of both Schwarzschild and RN BH which revealed that ModMax BH is more stable than the Schwarzschild and RN BH.

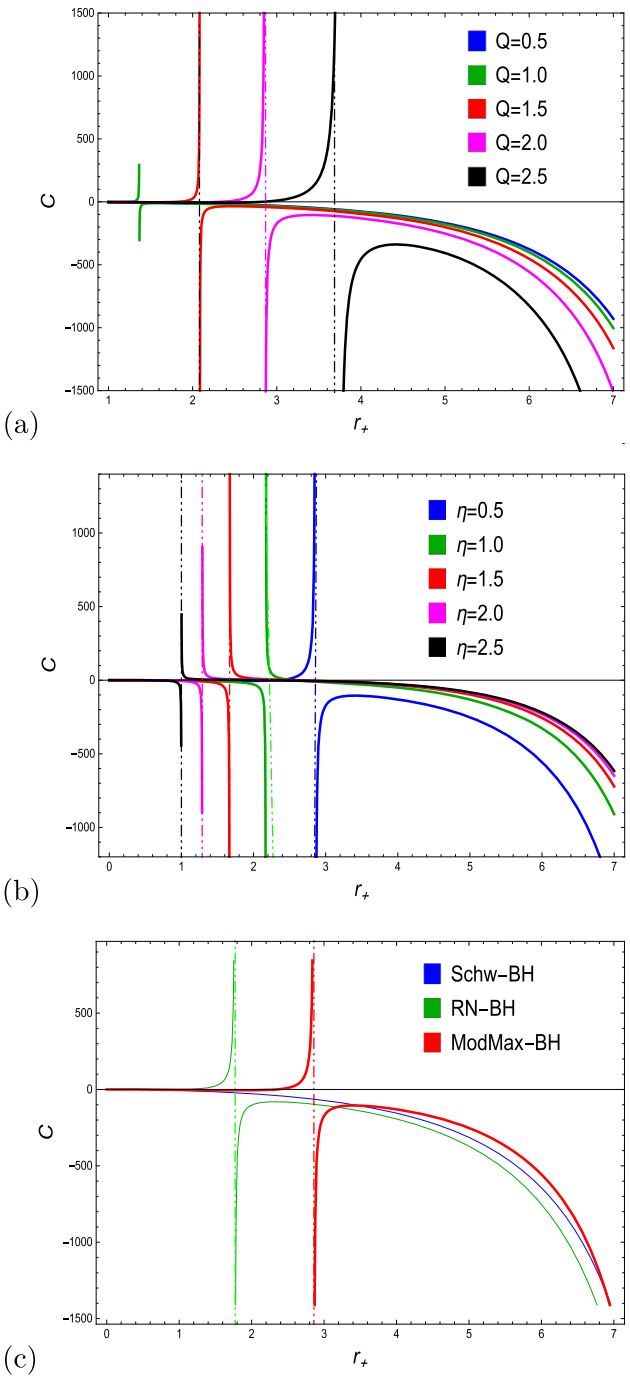

Fig. 4 Evolution of specific heat C along r_+ by taking $l = 15$, **a** $\eta = 0.50$ for different values of Q **b** for $Q = 2.00$ and different values of η and **c** represents the comparative analysis of the behavior of specific heat C for Schwarzschild BH (blue curve) with $\eta = 0$, $Q = 0$, RN-BH (green curve) with $\eta = 0$ and $Q \neq 0$ and red curve denotes the ModMax BH for which $\eta \neq 0$ and $Q \neq 0$

4 P–V criticals and critical exponents

In this section, we investigate the extended phase transition of Modmax AdS-BH [117] by involving the BH thermodynamic pressure. Later on by computing critical values of Modmax AdS-BH by the means of equation of state, we will sort out the critical exponents. In the extended phase space, the relationship between pressure and curvature in the context of thermodynamic considerations as follows

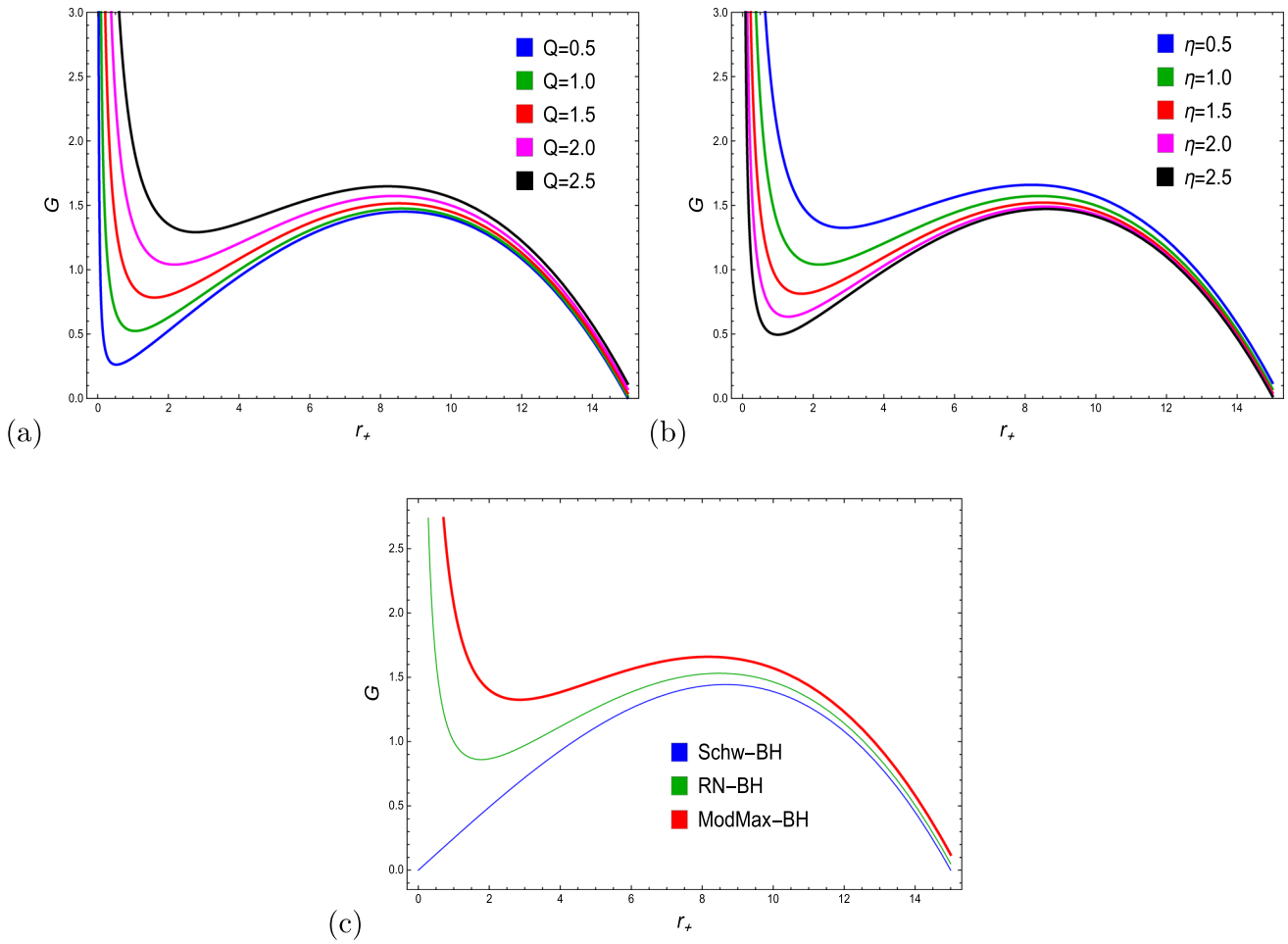

Fig. 5 Evolution of Gibbs free energy G along r_+ by taking $l = 15$, **a** $\eta = 1$ for different values of Q **b** for $Q = 2.00$ and different values of η and **c** represents the comparative analysis of the behavior of Gibbs free energy G for Schwarzschild BH (blue curve) with $\eta = 0$, $Q = 0$, RN-BH (green curve) with $\eta = 0$ and $Q \neq 0$ and red curve denotes the ModMax BH for which $\eta \neq 0$ and $Q \neq 0$

$$P = \frac{3}{8\pi l^2}, \tag{10}$$

Inserting Eq. (10) into Eq. (5), the equation of state becomes

$$P(r_+, T) = \left(\frac{Q^2 \exp(-\eta)}{8\pi r_+^4} + \frac{T}{2r_+} - \frac{1}{8\pi r_+^2}\right), \quad \tilde{V} = 2r_+. \tag{11}$$

Also,

$$P(\tilde{V}, T) = \left(\frac{2Q^2 \exp(-\eta)}{\pi \tilde{V}^4} + \frac{T}{\tilde{V}} - \frac{1}{2\pi \tilde{V}^2}\right). \tag{12}$$

There are two conditions to find critical values of Modmax AdS-BH, which are given below

$$\left(\frac{\partial P}{\partial r_+}\right)_T = 0 \quad || \quad \left(\frac{\partial^2 P}{\partial r_+^2}\right)_T = 0. \tag{13}$$

From Eqs. (11), and (13), determine the required critical values as,

$$r_c = \sqrt{6}\exp(-\frac{\eta}{2})Q, \tag{14}$$

$$V_c = 2\sqrt{6}Q\exp\left(-\frac{\eta}{2}\right), \tag{15}$$

$$T_c = \frac{\exp\left(\frac{\eta}{2}\right)}{3\sqrt{6}\pi Q}, \tag{16}$$

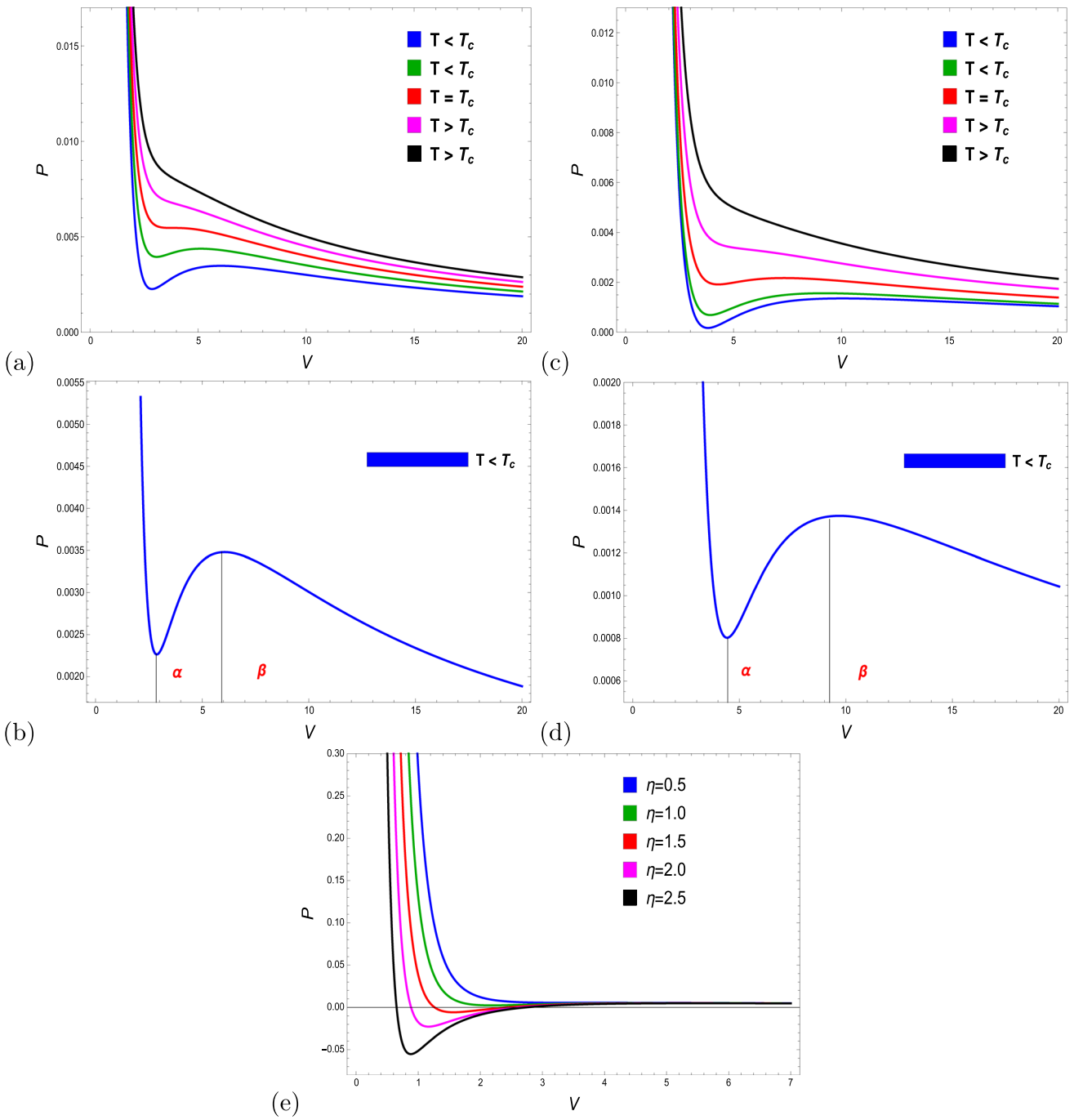

Fig. 6 Conduct of P–V criticality (i.e., plot of P along V), **a** for $\eta = 0.5$ and $Q = 1$ for different values of T (**b**) represents the stable and unstable regions corresponding to plot (**a**) and **c** for $\eta = 1$ and $Q = 1.8$ for different values of T **d** represents the stable and unstable regions corresponding to plot (**b**), **e** for $T = 0.056$ and $Q = 1$ for different values of η

$$P_c = \frac{\exp(\eta)}{96\pi Q^2}. \tag{17}$$

In order to observe the phase transitions and behavior of the NLED ModMax AdS BH, we create P–V diagrams using the volume, pressure, and temperature equations. It can be seen from Fig. 6 that when $T > T_c$, a thermodynamic system is stable and acts like an ideal gas. At the point where $T = T_c$, the isotherm exhibits an inflection, and in contrast, instability persists when $T < T_c$. In order to gain a deeper understanding, we direct our attention towards the phenomenon of a phase transition occurring in a small or large BH. Specifically, we analyze the behavior of a curve $T < T_c$, as depicted in Fig. 6b and d for cases (a) and (c) respectively. The manifestation of stability through phase transition becomes apparent when observing the domains denoted as $V \in [0, a]$ and

$[b, \infty]$, which leads to the small and large radii. In the region of $V \in [a, b]$, where instability manifests, the coexistence of phase transitions is observed for both the small and large BHs within the unstable domain. To demonstrate the influence of η on P–V criticality, we have Fig. 6e.

While computing the thermodynamic quantities, it is noticed that when a thermodynamic system undergoes a second-order phase transition, there exist universal parameters known as critical exponents. These critical exponents play a fundamental role in distinguishing the specific behavior near critical values. Remarkably, these critical exponents describe the important property of the BH, independent of the system parameters of critical exponents. In the neighborhood of the critical points, one can observe four critical exponents that identify the behavior of specific heat $\tilde{\alpha}$, $\tilde{\beta}$ the order parameter, $\tilde{\gamma}$ isothermal compressibility, and $\tilde{\delta}$ the critical isotherm. These critical exponents characterize phase transitions analogous to Vander Waals fluids. These critical exponents can be defined as follows:

$$C_V \propto |\tau|^{-\tilde{\alpha}}, \qquad \tilde{\eta} = V_s - V_l \propto |\tau|^{\tilde{\beta}}, \tag{18}$$

$$k\tau = \propto |\tau|^{-\tilde{\gamma}}, \qquad |P - P_c|_{T_c} \propto |V - V_c|^{\tilde{\delta}}. \tag{19}$$

Here C_V, $\tilde{\eta} = V_s - V_l$, and $k\tau$ are the specific heat at constant volume, the volume difference from small to large phases and isothermal compressibility, respectively. We define

$$\tau = \frac{T}{T_c} - 1 = t - 1, \Rightarrow t = 1 + \tau. \tag{20}$$

$$\omega = \frac{v}{v_c} - 1 = \phi - 1, \Rightarrow \phi = 1 + \omega. \tag{21}$$

$$p = \frac{P}{P_c}, \Rightarrow P = P_c p. \tag{22}$$

Now, we are going to transform equation of state (as given in Eq. (12)), into the associated form as

$$pP_c = \frac{Q^2 \exp(-\eta)}{8\pi\phi^4 V_c^4} + \frac{tT_c}{2\phi V_c} - \frac{1}{8\pi\phi^2 V_c^2}. \tag{23}$$

After some simplification and manipulation, we can get

$$p = \frac{8t}{3\phi} + \frac{1}{3\phi^4} - \frac{2}{\phi^2}, \tag{24}$$

$$t = \frac{3p\phi}{8} - \frac{1}{8\phi^3} + \frac{3}{4\phi}. \tag{25}$$

The above mentioned Eq. (25), is called equation of state in transform case. We obtained the transform expression after some manipulation by using Eqs. (20), and (21), as

$$p = 1 + \frac{8}{3}\tau - \frac{8}{3}\tau\omega - \frac{4}{3}\omega^3. \tag{26}$$

Taking derivative of Eq. (26), with respect to ω, we get

$$dP = -P_c\left(\frac{8}{3}\tau + 4\omega^2\right). \tag{27}$$

In BH thermodynamic system, the phase transitions undergoes from small phase to large phase by keeping pressure and temperature constant,whereas volume of the BH system change from ω_s to ω_l. From the Maxwell's area law ($\oint VdP = 0$), we obtain the following equation,

$$p = 1 + \frac{8}{3}\tau - \frac{8}{3}\tau\omega_s - \frac{4}{3}\omega_s^3 = 1 + \frac{8}{3}\tau - \frac{8}{3}\tau\omega_l - \frac{4}{3}\omega_l^3. \tag{28}$$

$$\int_{\omega_s}^{\omega_l} \omega dp = 0, \tag{29}$$

after certain calculation, one can get

$$\omega_l = -\omega_s = \sqrt{-\frac{4}{3}\tau}. \tag{30}$$

Now, we will compute all the four parameters of the critical exponents:

1- The C_V is governed by $\tilde{\alpha}$

$$\begin{aligned} C_V &= T\frac{\partial S}{\partial T}|_V \propto |\tau|^{-\tilde{\alpha}} \\ &\Rightarrow \frac{\partial S}{\partial T} = 0 \end{aligned}. \tag{31}$$

Hence heat capacity under constant volume is equal to zero, so we immediately conclude that $\tilde{\alpha} = 0$

2− Exponent $\tilde{\beta}$ describes $\tilde{\eta} = V_s - V_l$.

$$\tilde{\eta} = V_s - V_l \propto |\tau|^{\tilde{\beta}} \tag{32}$$

We can find the volume difference in order to find the value of $\tilde{\beta}$

$$\tilde{\eta} = V_s - V_l = V_c(1 + \omega_s) - V_c(1 + \omega_l), \tag{33}$$

which gives

$$\tilde{\eta} = 4V_c\sqrt{-\frac{4}{3}\tau}, \tag{34}$$

write the above equation as

$$\tilde{\eta} = 4V_c|\frac{-4}{3}\tau|^{\frac{1}{2}} \tag{35}$$

which implies that

$$\tilde{\beta} = \frac{1}{2}. \tag{36}$$

3- By the definition of isothermal compressibility $k\tau$ and Eq. (24), we have

$$k\tau = \frac{-1}{V}\frac{\partial V}{\partial P}|_T \propto |\tau|^{-\tilde{\gamma}}, \tag{37}$$

$$\Rightarrow \tilde{\gamma} = 1. \tag{38}$$

4− As $T = T_c$, governs critical isotherm,

$$|P - P_c|_{T_c} \propto |V - V_c|^{\tilde{\delta}}, \tag{39}$$

$$\tilde{\alpha} + \tilde{\beta}(\tilde{\delta} + 1) = 2, \tag{40}$$

which implies that $\tilde{\delta} = 3$. The obtained critical exponents demonstrate consistency with their corresponding analogues for the RN-AdS black hole [58]. The identical critical exponents were derived for many BH solutions within distinct theoretical frameworks. Hence, we can deduce that critical behavior exhibits certain universal characteristics, at least for the wide variety of black hole solutions across multiple independent frameworks.

5 Joule–Thomson expansion

This section delves into the well-known J–T expansion in thermodynamics [62, 63, 74]. Expansion always causes a decrease in pressure, while fluid temperature increases. The primary goal of this method is to determine the J–T coefficient.

$$\mu_j = \left(\frac{\partial T}{\partial P}\right)_H = \frac{\left(\frac{\partial T}{\partial r_+}\right)_H}{\left(\frac{\partial P}{\partial r_+}\right)_H} = \frac{1}{C_p}\left[\left(\frac{\partial V}{\partial T}\right)_P - V\right], \tag{41}$$

where μ_j is called J–T coefficient. The well-known J–T coefficient has been widely utilized to estimate temperature fluctuations and evaluate the cooling or heating of gases during adiabatic expansion. In the case where μ_j takes a positive value, the fluid undergoes a cooling process, and vice versa if the value of μ_j is negative.

The heat capacity $C_P = T\left(\frac{\frac{\partial S}{\partial r_+}}{\frac{\partial T}{\partial r_+}}\right)$, is given by

$$C_P = \frac{r_+^3 \exp(\eta)\left(16\pi^2 P r_+^3 + 1\right) - Q^2 r_+}{r_+^2 \exp(\eta)\left(8\pi P r_+^2 - 1\right) + 3Q^2}. \tag{42}$$

By utilizing the certain thermodynamical quantities, we obtained the J–T coefficient as

$$\mu_j = \frac{4\pi r_+^3\left(\frac{12\pi r_+^3 \exp(\eta)}{r_+^2 \exp(\eta)(8\pi P r_+^2 - 1) + 3Q^2} - 1\right)\left(r_+^2 \exp(\eta)\left(8\ \mathrm{P}\ \pi r_+^2 - 1\right) + 3Q^2\right)}{3\left(r_+^3 \exp(\eta)\left(16\pi^2 P r_+^3 + 1\right) - Q^2 r_+\right)}. \tag{43}$$

it is convenient to put $\mu_j = 0$ in Eq. (41) to get inversion temperature as

$$T_i = \frac{r_+}{3}\left(\frac{\partial T}{\partial r_+}\right). \tag{44}$$

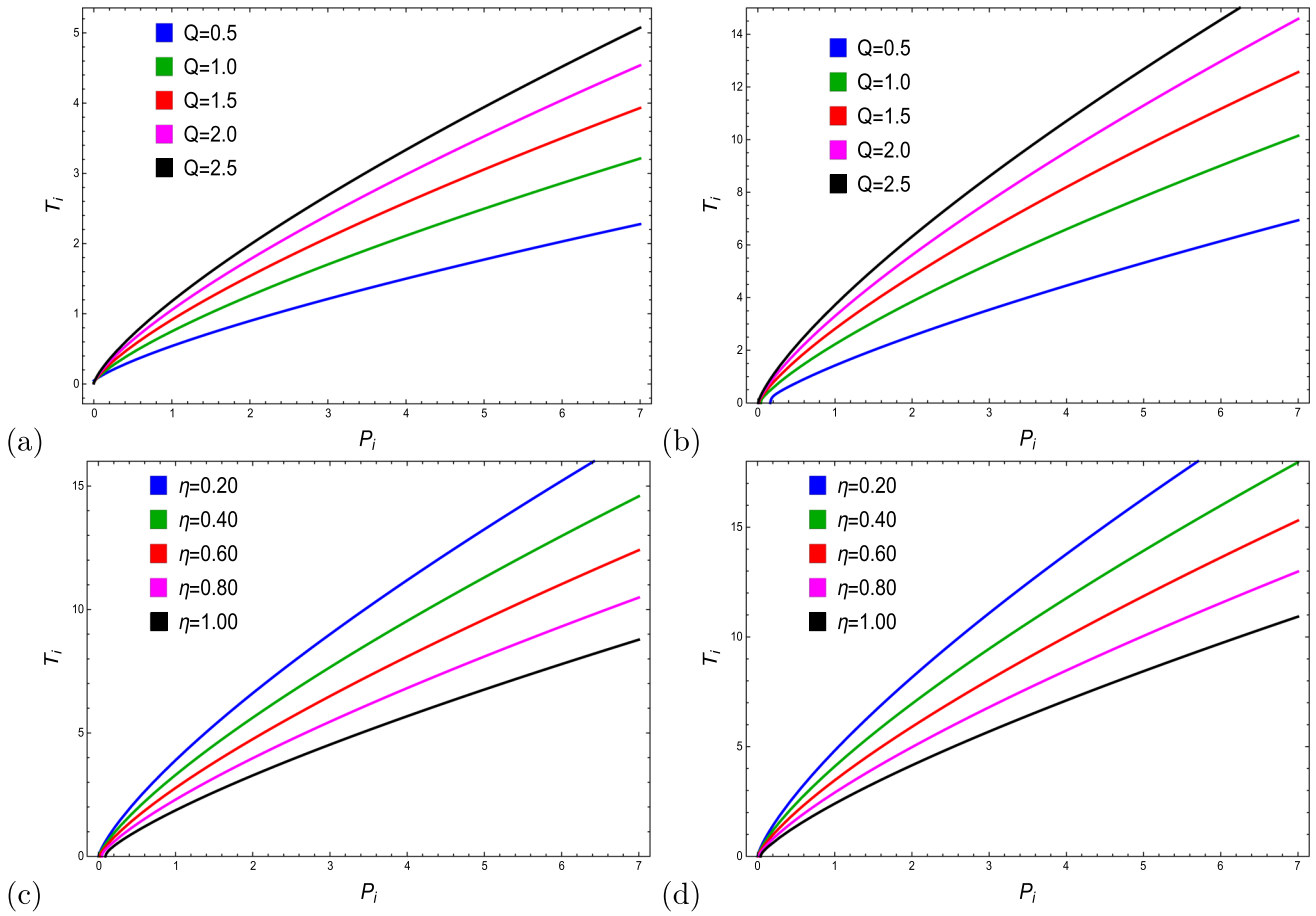

Fig. 7 Graphical conduct of inversion temperature T_i along P **a** $\eta = 0.2$ for different values of Q **b** for $\eta = 0.4$ and different values of Q and **c** $Q = 2$ for different values of η and **d** $Q = 3$ for different values of η

Implying Eqs. (5), (10), (11), and (44), one can obtain inversion pressure and inversion temperature as,

$$P_i = \Big(\frac{3Q^2\exp(-\eta)}{8\pi r_+^4} - \frac{1}{4\pi r_+^4}\Big), \tag{45}$$

and

$$T_i = \Big(\frac{Q^2\exp(-\eta)}{2\pi r_+^3} - \frac{1}{4\pi r_+}\Big). \tag{46}$$

In order to discuss the cooling and heating phases, the inversion curves $T_i - P_i$ have been plotted in Fig. 7, by taking a fixed value of the coupling parameter η with different values of the charge parameter Q ((a) $\eta = 0.2$ and (b) $\eta = 0.4$) and vice versa (Fig. 7c $Q = 2$ and d $Q = 3$). It can be observed that the inversion temperature is an increasing function of P_i. The effect of Q on inversion temperature is significant; as the value of Q grows, the inversion temperature turns larger. The prestige of the coupling parameter on the inversion temperature is in reverse order as in the case of charge parameter Q, i.e., T_i decreases with the increasing values of η.

The J–T expansion is a fascinating phenomenon wherein the enthalpy remains constant. It is of greater importance to delve into the graphical analysis of isenthalpic curves, specifically for the charged BH with NLED. The isenthalpic curves for the AdS-charged BH coupled with NLED are depicted in Fig. 8.

It can be observed that the slope of the isenthalpic curve remains positive in a specified region of the domain, identifying the cooling region. In contrast, after some extent, the slope of the isenthalpic curve changes its behavior and becomes negative, which indicates the heating region. The impact of the parameters Q and η is significant on the isenthalpic curves. One can note that as the charge Q increases, the temperature decreases, which indicates that the cooling and heating regions become smaller by fixing the value of η (see Fig. 8a–c). The influence of η is also important to identify the cooling and heating regions. We observe that for a fixed value of Q, as BH parameter η increases, the temperature also increases along the domain, inferring that the cooling and heating regions become larger (see Fig. 8 (d)-(f)).

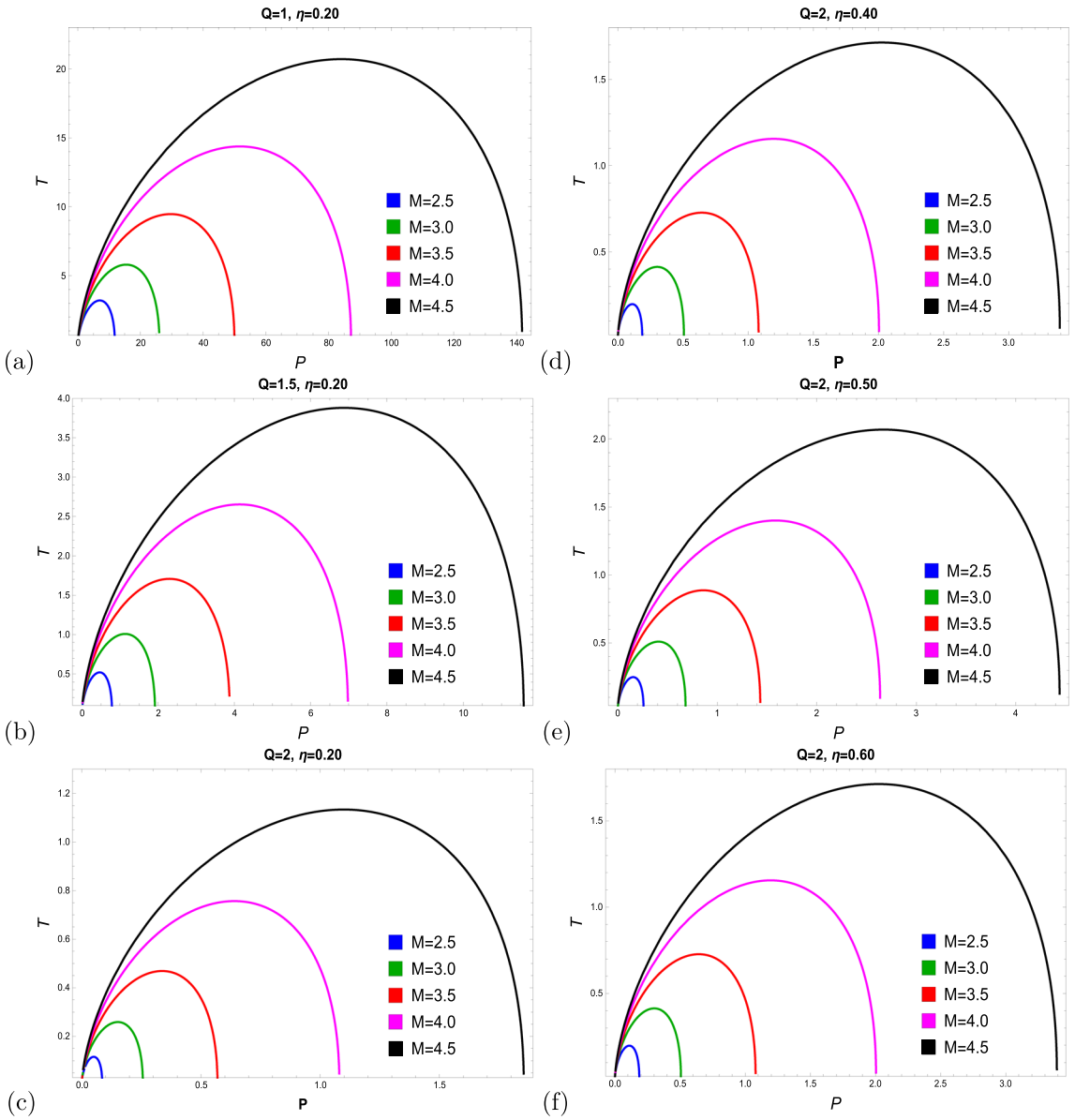

Fig. 8 Behavior of isenthalpic curves **a** for $\eta = 0.20$, $Q = 1.0$, **b** for $\eta = 0.20$, $Q = 1.5$, **c** for $\eta = 0.20$, $Q = 2.0$, **d** for $Q = 2.0$, $\eta = 0.40$, **e** for $Q = 2.0$, $\eta = 0.50$, and **f** for $Q = 2.0$, $\eta = 0.60$

It is noteworthy that the minimum inversion temperature can be obtained by implying $P = 0$,

$$T_i^{\min} = \frac{1}{6\sqrt{6}\pi\sqrt{Q^2\exp(-\eta)}}. \tag{47}$$

The ratio of inversion temperature to the critical temperature is

$$\frac{T_i^{\min}}{T_c} = \frac{e^{\eta/2}Q}{2\sqrt{e^{-\eta}Q^2}}. \tag{48}$$

If $\eta \to 0$, the ratio becomes

$$\frac{T_i^{\min}}{T_c} = \frac{1}{2}. \tag{49}$$

Table 1 The critical points of some BHs and the ratio of minimum inversion to the critical temperature

Type	The critical points	T_c	T_i^{min}	Ratio
Van der Waals fluids	Exist	$T_c = \frac{8a}{27kb}$	$T_i^{min} = \frac{2a}{9kb}$	$\frac{3}{4}$
Charged AdS RN BH	Exist	$T_c = \frac{1}{3\sqrt{6}\pi Q}$	$T_i^{min} = \frac{1}{6\sqrt{6}\pi Q}$	$\frac{1}{2}$
Charged AdS Torus-like BH	Not exist	Not exist	$T_i^{min} = 0$	Not exist
Charged AdS ModMax BH	Exist	$T_c =$ Appendix	$T_i^{min} =$ Appendix	$\frac{1}{2}$

6 Final remarks

The current study explored the thermal properties such as, geometrical mass of BH, Hawking temperature, heat capacity, Gibbs free energy, P–V criticality and critical exponents of AdS-ModMax BH coupled with NLED. The comparative analysis of these thermal properties of present study with the well known BHs, i.e., Schwarzschild and RN BHs is also presented. We have studied the J–T expansion which comprises, J–T coefficient, inversion temperature, inversion pressure and isenthalpic curves in order to reveal the cooling and heating regions of AdS-ModMax BH. In order to reveal the physical significance of these quantities, we have presented the graphical analysis. The salient traits of our findings are as follows:

- Horizon radius of AdS-ModMax BH lies between the horizon radii of Schwarzschild BH and RN-BH, which is greater than the RN-BH and less than the Schwarzschild BH.
- The mass of the BH increases monotonically along the radius for large value of the radius which indicates that BH absorbs energy from surrounding. The impact of the BH parameters on the mass of the BH is also notable, which manifesting that for larger value of the charge Q, BH absorbing more energy from surrounding and for greater values of the BH parameter η BH absorb less energy as compared to the smaller value of η. The comparative analysis revealed that the AdS-ModMax BH absorbed more energy than both Schwarzschild and RN BHs.
- The Hawking temperature for large radius increases monotonically along the radius revealing the endothermic process. For smaller value of Q and larger value of η the Hawking temperature is maximum.
- The local stability of the system revealed by the heat capacity. The heat capacity of the system diverges for large BH indicating the exothermic process.
- The global stability of the system is determined by the GFE. The GFE decreases monotonically along the horizon radius for large value of the radius but remain in the positive region indicating the global stability of the system. The GFE increases for increasing values of charge Q and decrease for increasing value of the BH parameter η.
- To observe the extended phase space, we rendered the P–V criticality. It is observed that when Hawking temperature is less than the critical temperature there exists instability in a specific domain $[\alpha, \beta]$. To clearly analyze the second order phase transition, the curves for $T < T_c$ is presented in Fig. 6b, d corresponding to the plots in (a) and (c) respectively. The impact of parameter η on the P–V criticality is interesting. For $\eta = 0.5$ and $\eta = 1.0$, P remains in the stable region and there is no phase transition, whereas for larger values of the parameter η, there can be a pase transition observed.
- The inversion temperature and isenthalpic curves demonstrated the cooling and heating regions as has been manifested in Figs. 7 and 8. The influences of the BH parameters η and Q have reflected from the corresponding plots.
- The comparative analysis of critical and inversion temperature for some well-known BHs has been presented in Table 1. Interestingly, it is quite possible to regain the well-known result of the AdS RN-BH from our studied AdS ModMax BH by considering the limit $\eta \to 0$.

In conclusion, we have analyzed the thermal aspects and J–T expansion of ModMax BH in detail. The comparative study of ModMax BH with the RN-BH and the Schwarzschild BH reveals the novelty of our considered BH. In comparison we have observed that the mass of ModMax BH is greater than RN BH and Schwarzshild BH. So, we conclude that increasing the mass of ModMax BH tends to enhance its stability by strengthening its gravitational influence, enlarging its event horizon, and promoting more stable interactions with its surrounding environment rather than RN and Schwarzshild BHs. It is worthwhile to note that positive and negative Hawking temperatures imply the physical and non-physical solutions, while stability and instability of the BH system are demonstrated by specific heat and free energy. Our result shows that as the Hawking temperature exceed from critical temperature, the corresponding thermodynamical pressure becomes maximum. We have estimated the fluctuations in temperature and appraised the cooling-heating process during expansion, through the value of the J–T coefficient which shows that the negative (positive) sign of the J–T coefficient yield the heating (cooling) process. Hence, ModMax BH parameters η have significant impact on the thermodynamical quantities in comparison with RN BH and Schwarzshild BH.

The work presented in this article can be extended to many extents. It would be interesting to explore some topological classes of static and rotating Modmax BH thermodynamics. Different techniques such as: Euclidean thermodynamics, Hamiltonian ther-

modynamics, Dynamic phase transition, Wald procedure, multi-critical points, light ring images, the optical appearance and the process of heat engines can also be employed on the considered BH.

Data Availability Statement No Data associated in the manuscript.

Appendix A

$$T_{\rm c} = \frac{\exp\left(\frac{\eta}{2}\right)}{3\sqrt{6}\pi Q}. \tag{50}$$

$$T_i^{\min} = \frac{1}{6\sqrt{6}\pi\sqrt{Q^2\exp(-\eta)}}. \tag{51}$$

References

1. H. Reissner, Ann. Phys. (Berlin) **50**(9), 106 (1916)
2. H. Weyl, Ann. Phys. (Berlin) **54**(18), 117 (1917)
3. G. Nordstrm, Verhandl Koninkl, Ned Akad, Wetenschap Afdel. Natuurk. Amsterdam **26**, 1201 (1918)
4. G.B. Jeffery, Proc. R. Soc. Lond. A. **99**(697), 123 (1921)
5. L.J. Romans, Nucl. Phys. B **383**, 395 (1992)
6. J.D. Bekenstein, Lett. Nuov. Cim. **4**, 737 (1972)
7. J.D. Bekenstein, Phys. Rev. D **7**, 949 (1973)
8. S.W. Hawking, Commun. Math. Phys. **43**, 199 (1975)
9. S.W. Hawking, Phys. Rev. D **13**, 191 (1976)
10. J.E. Aman, I. Bengtsson, N. Pidokrajt, Gen. Relativ. Gravit. **35**, 1733 (2003)
11. B.P. Dolan, Class. Quantum Grav. **28**, 235017 (2011)
12. S. Carlip, Int. J. Mod. Phys. D **23**(11), 1430023 (2014)
13. D. Kubiznak, R.B. Mann, Can. J. Phys. **93**(9), 999 (2014)
14. A. Kumar, S.G. Ghosh, S.D. Maharaj, Phys. Dark Univ. **30**, 100634 (2020)
15. V.V. Kiselev, Class. Quantum Grav. **20**, 1187 (2003)
16. Y.H. Wei, Z.H. Chu, Chin. Phys. Lett. **28**, 100403 (2011)
17. K. Ghaderi, B. Malakolkalami, Grav. Cosmol. **24**, 61 (2018)
18. K. Ghaderi, B. Malakolkalami, Astrophys. Space Sci. **361**, 161 (2016)
19. F. Liu, L.C. Zhang, Chin. J. Phys. **57**, 53 (2019)
20. R. Ndongmo, S. Mahamat, T. Bouetou Bouetou, T. Crepin Kofane, Phys. Scr. **96**(9), 095001 (2021)
21. Y. Zhang, Y.B. Ma, Y.Z. Du, H.F. Li, L.C. Zhang, Eur. Phys. J. C **82**, 770 (2022)
22. R. Penrose, Phys. Rev. Lett. **14**, 57 (1965)
23. S. Hawking, R. Penrose, Proc. R. Soc. Lond. A. **314**, 529 (1970)
24. A.D. Sakharov, Sov. Phys. JETP **22**, 241 (1966)
25. E.B. Gliner, Sov. Phys. JETP **22**, 378 (1966)
26. S.A. Hayward, Phys. Rev. Lett. **96**, 031103 (2006)
27. M.H. Li, K.C. Yang, Phys. Rev. D **86**, 123015 (2012)
28. S.G. Ghosh, Eur. Phys. J. C **75**, 532 (2015)
29. H. Culetu, Int. J. Theor. Phys. **54**, 2855 (2015)
30. V.P. Frolov, Phys. Rev. D **94**, 104056 (2016)
31. K.S. Stelle, Phys. Rev. D **16**, 953 (1977)
32. K.S. Stelle, Gen. Relat. Gravit. **9**, 353 (1978)
33. D.I. Kazakov, S.N. Solodukhin, Nucl. Phys. B **429**, 153 (1994)
34. T. Biswas, E. Gerwick, T. Koivisto, A. Mazumdar, Phys. Rev. Lett. **108**, 031101 (2012)
35. S.G. Ghosh, R.K. Walia, Ann. Phys. **434**, 168619 (2021)
36. B. Pourhassan, Eur. Phys. J. C **79**, 740 (2019)
37. B. Pourhassan, M. Faizal, Eur. Phys. J. C **77**, 96 (2017)
38. B. Pourhassan, S. Upadhyay, Eur. Phys. J. Plus **136**, 311 (2021)
39. B. Pourhassan, M. Faizal, U. Debnath, Eur. Phys. J. C **76**, 145 (2016)
40. B. Pourhassan, M. Faizal, Phys. Lett. B **755**, 444–45 (2016)
41. A. Dehghani, B. Pourhassan, S. Zarepour, E.N. Saridakis, Phys. Dark Univ. **42**, 101371 (2023)
42. R.H. Ali, G. Abbas, Chin. Phys. C **47**, 11 (2023)
43. R.H. Ali, G. Abbas, Chin. J. Phys. **85**, 386–401 (2023)
44. G. Abbas, R.H. Ali, Chin. Phys. C **47**, 065103 (2023)
45. G. Abbas, R.H. Ali, Eur. Phys. J. C **83**, 407 (2023)
46. B. Pourhassan, K. Kokabi, Z. Sabery, Ann. Phys. **399**, 181 (2018)
47. S.H. Hendi, B. Esla, S. Panahiyan et al., Phys. Lett. B **767**, 214–225 (2017)
48. B. Pourhassan, H. Farahani, S. Upadhyay, Int. J. Mod. Phys. A **34**, 1950158 (2019)
49. A. Jawad, Class. Quantum Grav. **37**, 185020 (2020)
50. M. Sharif, A. Khan, Chin. J. Phys. **77**, 1130 (2022)
51. M. Sharif, Z. Akhtar, Phys. Dark Univ. **29**, 100589 (2020)
52. M. Sharif, A. Khan, Chin. J. Phys. **77**, 1885–1902 (2022)

53. B. Pourhassan, S. Upadhyay, Eur. Phys. J. plus **136**, 311 (2021)
54. S.G. Ghosh, A. Kumar, D.V. Singh, Phys. Dark Univ. **30**, 100660 (2020)
55. D.V. Singh, S.G. Ghosh, S.D. Maharaj, Phys. Dark Univ. **30**, 100730 (2020)
56. S.G. Ghosh, D.V. Singh, R. Kumar, S.D. Maharaj, Ann. Phys. **424**, 168347 (2021)
57. S.G. Ghosh, D.V. Singh, S.D. Maharaj, Phys. Rev. D **97**(10), 104050 (2018)
58. A. Jawad, G. Abbas, I. Siddique, G. Mustafa, Eur. Phys. J. Plus. **137**, 284 (2022)
59. A. Jawad, A. Khawer, Eur. Phys. J. C **78**, 837 (2018)
60. X. Kong, Z. Zhang, L. Zhao, Chin. Phys. C **47**, 095105 (2023)
61. M.B. Ahmed, W. Cong, D. Kubiznak, R.B. Manna, M.R. Vissere, J. High Energy Phys. **08**, 142 (2023)
62. O. Okcu, E. Aydner, Eur. Phys. J. C **78**, 123 (2018)
63. M. Chabab, H. ElMoumni, S. Iraoui, K. Masmar, S. Zhizeh, LHEP **02**, 05 (2018)
64. J.X. Mo, G.Q. Li, S.Q. Lan, X.B. Xu, Phys. Rev. D **98**(12), 124032 (2018)
65. J.X. Mo, G.Q. Li, Class. Quantum. Grav. **37**, 045009 (2020)
66. S.Q. Lan, Phys. Rev. D **98**, 084014 (2018)
67. M. Chabab, H. El Moumni, S. Iraoui, K. Masmar, S. Zhizeh, Lett. High Energy Phys. **02**, 05 (2018)
68. X.M. Kuang, B. Liu, A. Ovgun, Eur. Phys. J. C **78**, 840 (2018)
69. J. Sadeghi, R. Toorandaz, Nucl. Phys. B **951**, 114902 (2020)
70. H. Ghaffarnejad, E. Yaraie, Phys. Lett. B **785**, 105–111 (2018)
71. X.M. Kuang, B. Liu, A. Ovgun, Eur. Phys. J. C **78**, 840 (2018)
72. Z.W. Zhao, Y.H. Xiu, N. Li, Phys. Rev. D **98**(12), 124003 (2018)
73. S.Q. Lan, Nucl. Phys. B **948**, 114787 (2019)
74. S.I. Kruglov, Nucl. Phys. B **984**, 115949 (2022)
75. S.I. Kruglov, Grav. Cosmol. **29**, 57–61 (2023)
76. P. Paul, S. Upadhyay, D. Veer Singh, Eur. Phys. J. Plus **138**, 6 (2023)
77. Y. Guo, H. Xie, Y. Gang-Miao, Nucl. Phys. B **993**, 116280 (2023)
78. D.J. Gogoi, Y. Sekhmani, D. Kalita, N.J. Gogoi, J. Bora, Fortschrit. Der Physik **71**, 2300010 (2023)
79. Y.-Z. Du, X. Liu, Y. Zhang, L. Zhao, Q. Gu, Eur. Phys. J. C **83**, 426 (2023)
80. N. Li, J. Li, B.Y. Su, Fortschrie der Physik **71**, 2200166 (2023)
81. M. Yasir, X. Tiecheng, F. Javed, G. Mustafa. https://doi.org/10.48550/arXiv.2305.13709
82. M. Yasir, X. Tiecheng, F. Javed, and G. Mustafa. https://doi.org/10.48550/arXiv.2305.13709
83. K.A. Bronnikov, I.G. Dymnikova, E. Galaktionov, Class. Quantum Grav. **29**, 095025 (2012)
84. S.V. Bolokhov, K.A. Bronnikov, M.V. Skvortsova, Class. Quantum Grav. **29**, 245006 (2012)
85. K.A. Bronnikov, K.A. Baleevskikh, M.V. Skvortsova, Phys. Rev. D **96**, 124039 (2017)
86. S. Nojiri, S.D. Odintsov, Phys. Rev. D **96**, 104008 (2017)
87. C. Gao, Y. Lu, S. Yu, Y. Shen, Phys. Rev. D **97**, 104013 (2018)
88. S. Gunasekaran, R.B. Mann, D. Kubiznak, J. High Energy Phys. **2012**, 110 (2012)
89. S.I. Kruglov, Nucl. Phys. B **984**, 115949 (2022)
90. Y.Z. Du, X. Liu, Y. Zhang, L. Zhao, Q. Gu, Eur. Phys. J. C **83**, 426 (2023)
91. S. Bi, M. Du, J. Tao, F. Yao, Chin. Phys. C **45**, 025109 (2021)
92. I. Bandos, K. Lechner, D. Sorokin, P.K. Townsend, Phys. Rev. D **102**, 121703 (2020)
93. A. Banerjee, A. Mehra, Phys. Rev. D **106**, 085005 (2022)
94. M.J. Neves, P. Gaete, L.P.R. Ospedal, J.A. Helayel-Neto, Phys. Rev. D **107**, 075019 (2023)
95. C.A. Escobar, R. Linares, Phys. Rev. D **106**, 036027 (2022)
96. I. Bandos, K. Lechner, D. Sorokin, P. Townsend, J. High Energy Phys. **2021**, 1–42 (2021)
97. I. Bandos, K. Lechner, D. Sorokin et al., J. High Energy Phys. **2021**, 31 (2021)
98. J. Barrientos, A. Cisterna, D. Kubiznak, J. Oliva, Phys. Lett. B **834**, 137447 (2022)
99. A. Ballon Bordo, D. Kubiznk, T. Perche, Phys. Lett. B **817**, 136312 (2021)
100. A. Bokulic, I. Smolic, T. Juric, Phys. Rev. D **103**, 124059 (2021)
101. R.C. Pantig, L. Mastrototaro, G. Lambiase, A. Ovgun, Eur. Phys. J. C **82**, 1155 (2022)
102. H. Babaei-Aghbolagh, K.B. Velni, D.M. Yekta, H. Mohammadzadeh, Phys. Rev. D **106**, 086022 (2022)
103. K. Lechner, P. Marchetti, A. Sainaghi, D.P. Sorokin, Phys. Rev. D **106**, 016009 (2022)
104. M. Ortaggio, Theor. Phys. **82**, 1056 (2022)
105. H. Nastase, Phys. Rev. D **105**, 105024 (2022)
106. C. Ferko, L. Smith, G.T. Mazzucchelli, Sci. Post Phys. **13**, 012 (2022)
107. A. Ali, K. Saifullah, Ann. Phys. **437**, 168726 (2022)
108. S.I. Kruglov, Int. J. Mod. Phys. D **31**, 2250025 (2022)
109. C.A. Escobar, R. Linares, B. Tlatelpa-Mascote, Int. J. Mod. Phys. A **37**, 2250011 (2022)
110. A. Bokulic, T. Juric, I. Smolic, Phys. Rev. D **105**, 024067 (2022)
111. K. Nomura, D. Yoshida, Phys. Rev. D **105**, 044006 (2022)
112. M. Zhang, J. Jiang, Phys. Rev. D **104**, 084094 (2021)
113. S.I. Kruglov, Phys. Lett. B **822**, 136633 (2021)
114. D.F. Alfonso, R. Linares, M. Maceda, JHEP **09**, 104 (2021)
115. H. Babaei-Aghbolagh, K.B. Velni, D.M. Yekta, H. Mohammadzadeh, Phys. Lett. B **829**, 137079 (2022)
116. D. Flores-Alfonso, B.A. Gonzalez-Morales, R. Linares, M. Maceda, Phys. Lett. B **812**, 136011 (2021)
117. B.P. Kosyakov, Phys. Lett. B **810**, 135840 (2020)